Non-Interferometric Testing

Introduction

In these notes four non-interferometric tests are described: (1) the Shack-Hartmann test, (2) the Foucault test, (3) the wire test, and (4) the Ronchi test. Unlike most interferometric tests, these four tests measure the slope of the wavefront error, rather than the wavefront error itself. The Shack-Hartmann test is especially useful for testing large telescope mirrors since if it is performed properly, atmospheric turbulence introduces little error into the test results. The Foucault test is a powerful method for qualitatively detecting small errors in optics, and it is simple and inexpensive to perform. The wire test is a modification of the Foucault test that makes it easier to obtain quantitative results. The Ronchi test can be thought of as a multiple wire test. While the Ronchi test will give many beautiful test results, the accuracy of the results is severely limited by diffraction.

8.2.11 Shack-Hartmann Test

The Shack-Hartmann test is essentially a geometrical ray trace that measures angular, transverse, or longitudinal aberrations from which numerical integration can be used to calculate the wavefront aberration.

Figure 1 illustrates the basic concept for performing a classical Hartmann test. A Hartmann screen, which consists of a plate containing an array of holes, is placed in a converging beam of light produced by the optics under test. One or more photographic plates or solid-state detector arrays are placed in the converging light beam after the Hartmann screen. The positions of the images of the holes in the screen as recorded on the photographic plates or detector arrays give the transverse and longitudinal ray aberrations directly. It should be noted that if a single photographic plate or detector array is used, both the hole positions in the screen and the distance between the screen and plate must be known, while if two photographic plates or detector arrays are used, only the distance between the plates or detector arrays need be known.

One advantage of the Hartmann test for the testing of telescope mirrors is that effects of air turbulence will average out. Air turbulence will cause the spots to wander, but as long as the integration time is long compared to the period of the turbulence the major effect will be for the spots to become larger, and as long as the centroid of the spots can be accurately measured the turbulence will not introduce error in the measurement. The holes in the Hartmann screen should be made large enough so diffraction does not limit the measurement accuracy, but not so large that surface errors are averaged out.

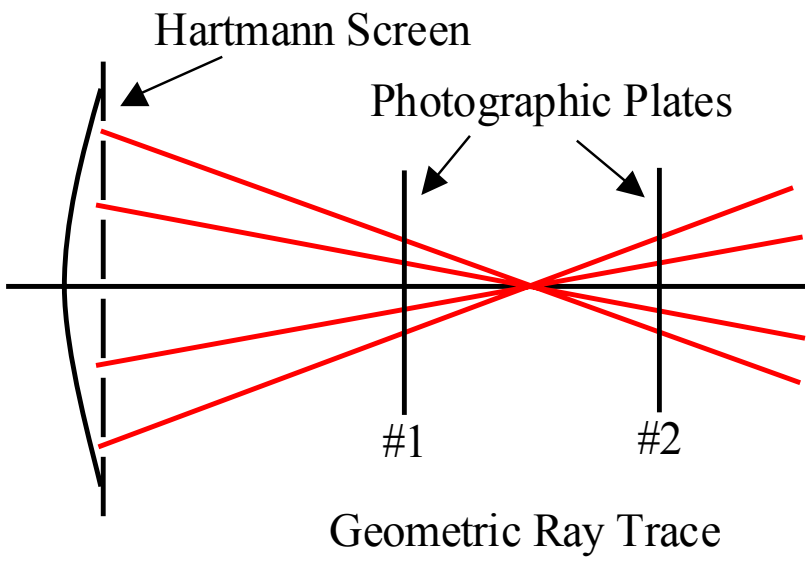

Fig. 1. Classical Hartmann test. Single photographic plate: must know (a) hole positions in screen, (b) distance between screen and plate. Multiple photographic plates: must know the distance between plates.

Figure 2 shows the results for testing a parabolic mirror at the center of curvature. Note that the detectors must be kept away from the caustic or much confusion can result. Once the transverse or longitudinal aberration is determined, the wavefront aberration can be determined.

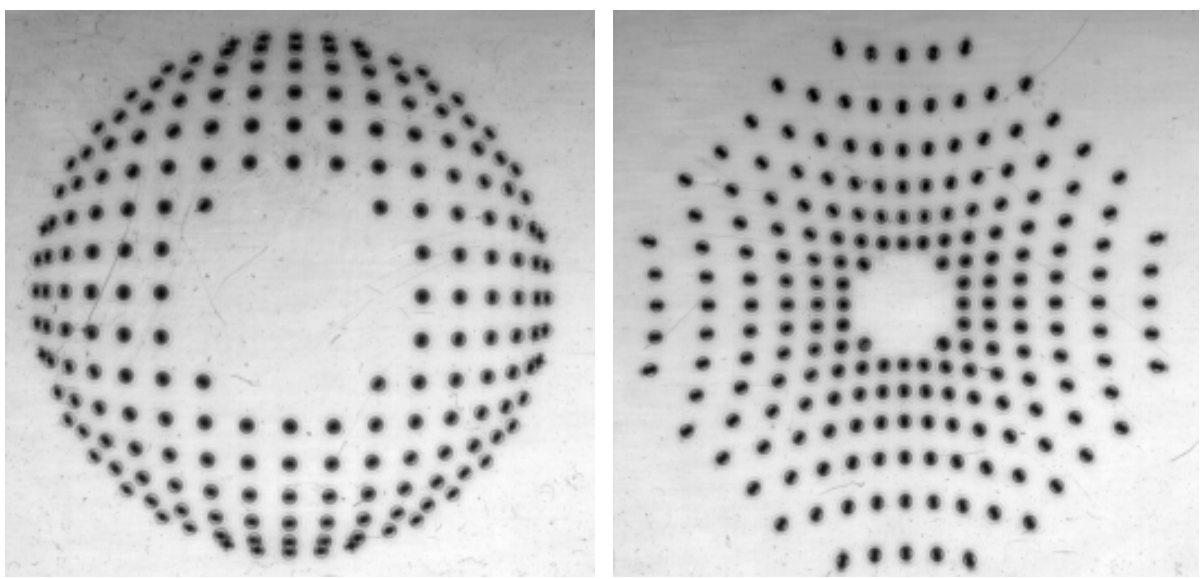

Outside Position **Inside Position**

Fig. 2. Hartmann test of parabolic mirror near center of curvature.

Shack modified the Hartmann test by replacing the screen containing holes with a lenslet array. In typical use the beam from the telescope is collimated and reduced to a size of a few centimeters and impinges on a lenslet array that focuses the light onto a detector array as shown in Figure 3. The positions of the various focused points give the local slope of the wavefront. Figure 4 shows photos of a Shack-Hartmann lenslet array.

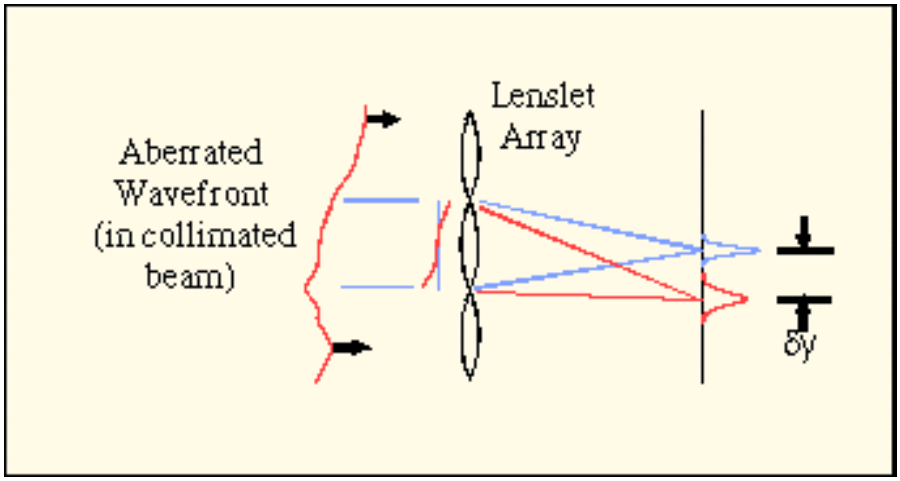

Fig. 3. Shack-Hartmann lenslet array measuring slope errors in an aberrated wavefront.

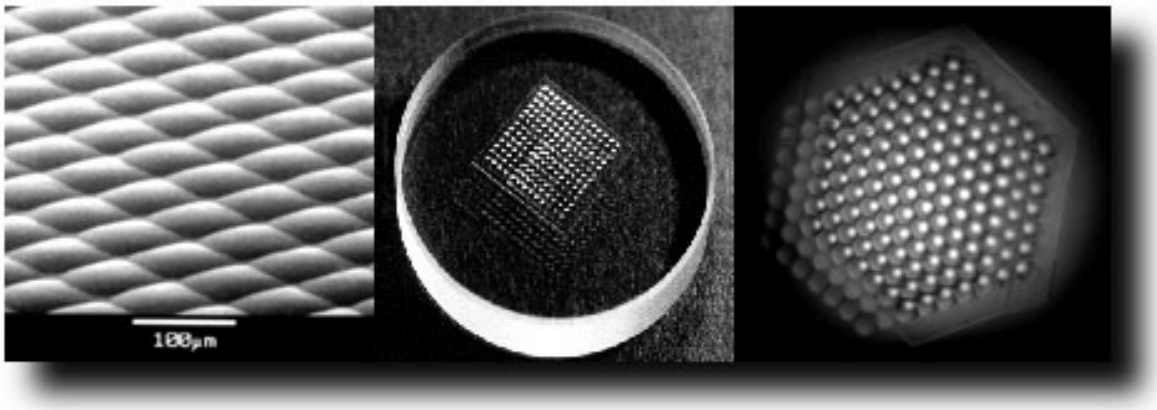

Fig. 4. Photos of a Shack-Hartmann lenslet array.

The Shack-Hartmann wavefront sensor is widely used in adaptive optics correction of atmospheric turbulence. Figure 5 shows a movie of the focused spots from the Shack-Hartmann test dancing around due to atmospheric turbulence.

Sh.mpeg

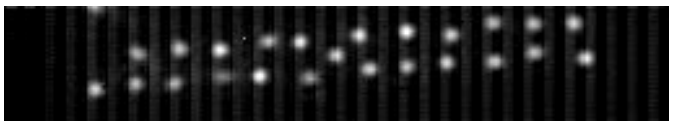

Fig. 5. Movie made using Shack-Hartmann test to measure atmospheric turbulence.

8.2.12 Foucault Test

The Foucault knife-edge test is one of the oldest and most common tests for determining longitudinal and transverse aberrations from which the wavefront aberration can be determined. In the Foucault test, a knife edge placed in the image plane is passed through the image of a point or slit source. The observer's eye is placed immediately behind the edge and allowed to focus upon the exit pupil of the system under test, as shown in Fig. 6 for testing a concave mirror. As the knife edge passes through the image, a shadow is seen to pass across the pupil. The more compact the light distribution in the image, the more rapidly the shadow passes across the pupil.

A perfect lens will have one image point such that the entire pupil of the lens is seen to darken almost instantaneously when the knife edge is passed through the image. If the knife edge is moved longitudinally toward the lens from this image point and again passed across the image, the shadow will be seen to travel across the aperture in the same direction in which the knife edge is passed across the image, as illustrated in Fig. 7. When the knife edge is located behind the point image, an opposite motion of the shadow occurs. The ultimate sensitivity of the test is attained by observing the motion of the shadow within certain zones of the aperture as the knife edge is cut across the image. In practice, the knife edge is most often used to measure the zonal focus of different parts of an optical surface. This information is of greatest interest to an optician who generally wants to know where the high and low parts of a surface are.

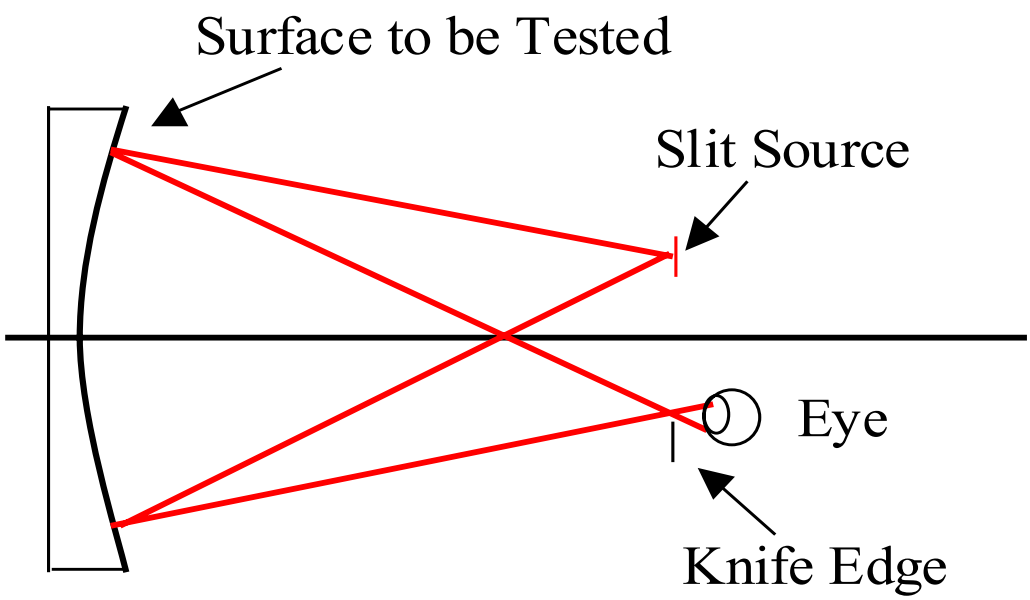

Fig. 6. Foucault knife-edge test.

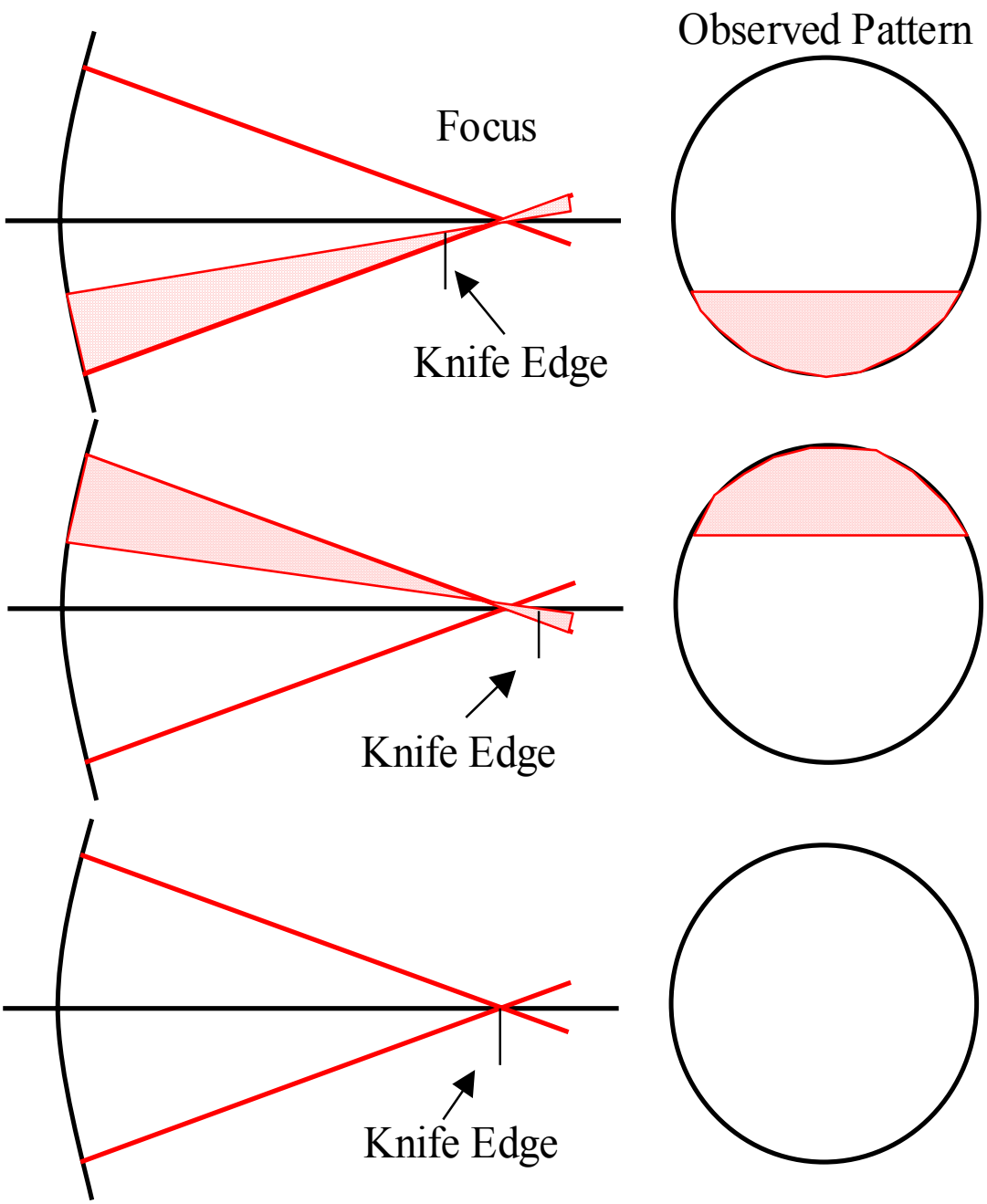

Fig.7. Ray picture of the Foucault knife-edge test.

It is not possible to describe in words the appearance of a Foucault shadow pattern for testing a general optical system. The Foucault shadows have to be observed to appreciate the sensitivity of the test for observing small slope errors; however, it is possible to describe the shadows that are obtained for the Seidel aberrations. It must be noted that the following is simply a geometrical analysis, and due to diffraction, the shadows are not as distinct as described below.

First, let us look at the shadows produced for third-order spherical aberration. For spherical aberration and defocus

$$\Delta W = W_{040}\,(x^2 + y^2)^2 + \frac{\epsilon_z\, h^2}{2\, R^2}\,(x^2 + y^2)\,.$$

The boundary of the geometrical shadow is obtained by setting the distance of the knife edge from the optical axis, d, equal to the transverse aberration for spherical aberration. Thus, for normalized pupil coordinates, the equation of the boundary of the shadow is

$$d = -\frac{R}{h}\,\frac{\partial\,\Delta W}{\partial\, y} = \frac{-4\,R\,W_{040}\,y\,(x^2 + y^2)}{h} - \frac{\epsilon_z\, h\, y}{R}\,; \tag{1}$$

Let us suppose, for a moment, that the knife edge is located on the optical axis, so d = 0. The solution to Eq. (1) then becomes

$$y = 0 \tag{2}$$

and

$$x^2 + y^2 = -\frac{\epsilon_z\, h^2}{4\, R^2\, W_{040}} \tag{3}$$

The first solution is the equation of a straight line through the origin, and the second solution is the equation of a circle of radius

$$\rho = \left(\frac{-\epsilon_z\, h^2}{4\, R^2\, W_{040}}\right)^{1/2} \tag{4}$$

The complete solution is illustrated in Fig. 8 for different values of ϵ_z. A procedure for finding W_{040} is to first find the paraxial focus by noting the position where the central spot in the pattern just vanishes. By measuring ρ as a function of ϵ_z, we obtain a measurement of W_{040} using Eq. (4).

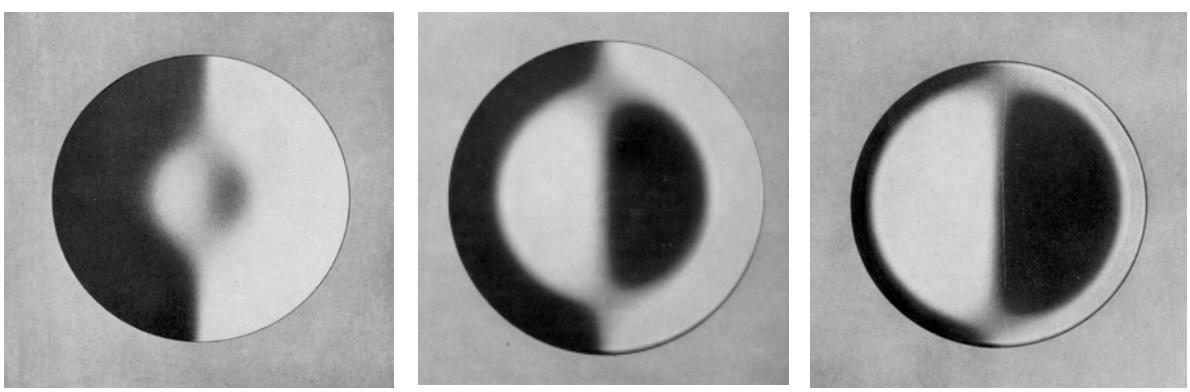

Knife edge near paraxial focus | Knife edge partway between paraxial and marginal focus | Knife edge near marginal focus

Fig. 8. Knife-edge test patterns due to third-order spherical aberration, when the knife edge is on the optical axis.

If the knife edge is not located on the optical axis, the simplified solutions given in Eq. (3) are not valid, and the cubic Eq. (1) must be considered. Drawings showing typical solutions are shown in Fig. 9.

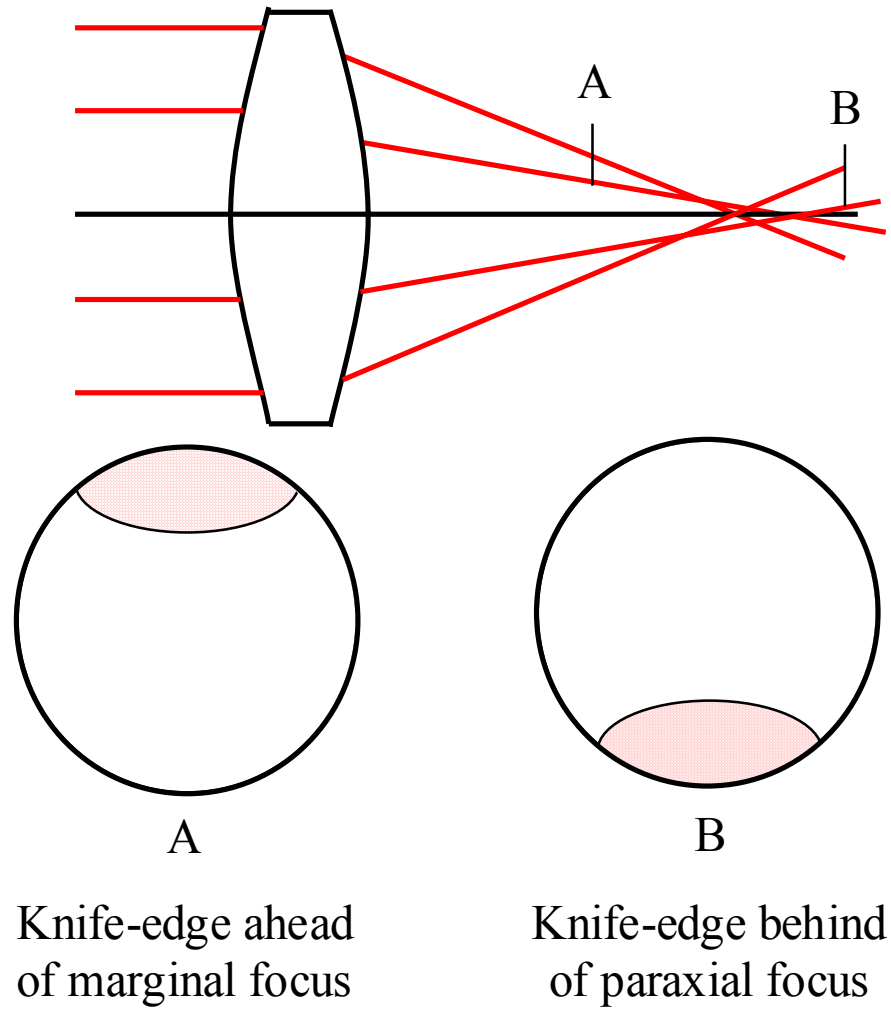

Fig. 9. Knife-edge test pattern for third-order spherical when knife-edge is not on the optical axis.

Next, we will consider the knife edge test for coma. For coma and defocus

$$\Delta W = W_{131}\, y_o\, y\, (x^2 + y^2) + \frac{\epsilon_z\, h^2}{2\, R^2}\, (x^2 + y^2)$$

Because of the asymmetry of coma, the pattern depends upon whether the knife edge is parallel to the x or the y axis. If the <u>knife edge is parallel to the x axis</u>, the equation of the boundary of the shadow is

$$d = -\frac{R}{h}\, \frac{\partial\, \Delta W}{\partial\, y} = -\frac{R}{h}\, W_{131}\, y_o\, (x^2 + 3\, y^2) - \frac{\epsilon_z\, h\, y}{R} \qquad (5)$$

which is the equation of an <u>ellipse</u>, while if the <u>knife edge is parallel to the y axis</u>, the equation of the boundary of the shadow is

$$d = -\frac{R}{h}\frac{\partial \Delta W}{\partial x} = -\frac{2R}{h} W_{131}\, y_o\, x\, y - \frac{\epsilon_z\, h\, x}{R} \qquad (6)$$

which is the equation of a hyperbola. Drawings showing typical test patterns for coma are shown in Fig. 10.

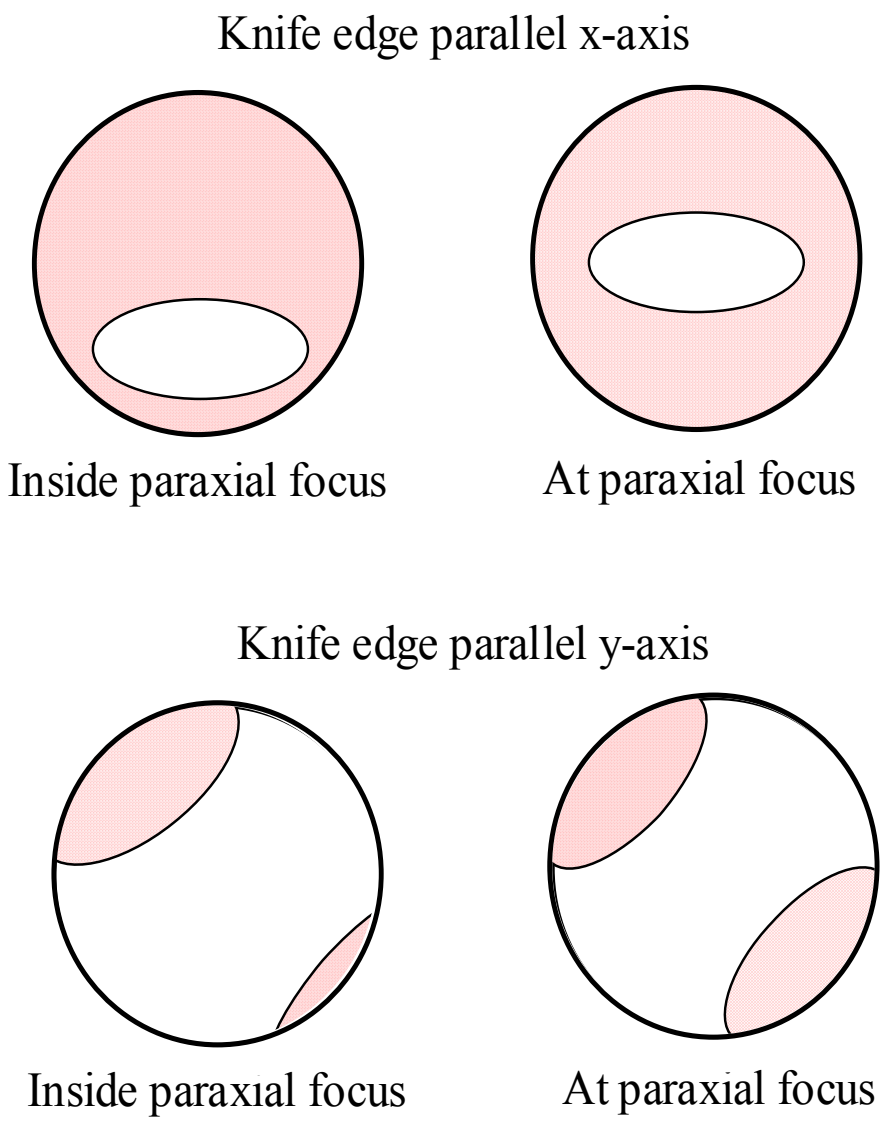

Fig. 10. Knife-edge test pattern due to coma.

The knife-edge test can be used to measure astigmatism in a lens. For astigmatism

$$\Delta W = W_{222}\, y_o^2\, y^2 + \frac{\epsilon_z\, h^2}{2\, R^2}\,(x^2 + y^2)$$

It is important that the knife edge is not parallel to either the tangential or the sagittal plane while making the measurement. If the knife edge is parallel to either the y or the x axis, the equations for the shadow boundaries would be

$$d = -\frac{R}{h}\frac{\partial \Delta W}{\partial x} = -\frac{\epsilon_z h}{R} x$$

or

$$d = -\frac{R}{h}\frac{\partial \Delta W}{\partial y} = -\left(\frac{2R}{h} W_{222} y_o^2 + \frac{\epsilon_z h}{R}\right) y \qquad (7)$$

which are just the equations of straight lines, so the astigmatic wavefront would be indistinguishable from a spherical wavefront. However, if we put the knife edge in the beam at an angle to the x axis, then d =- ϵ_x Sin[α] + ϵ_y Cos[α]. Therefore

$$d = \frac{\epsilon_z h}{R} x \operatorname{Sin}[\alpha] - \left(\frac{2R}{h} W_{222} y_o^2 + \frac{\epsilon_z h}{R}\right) y \operatorname{Cos}[\alpha] \qquad (8)$$

Hence, the angle of the shadow is not generally the same as the knife edge, and the angle changes as the knife edge is moved along the axis.

To measure the longitudinal aberration, it is convenient to place over the surface being tested a mask having two symmetrically located apertures to define the zone being measured. The knife edge is then shifted longitudinally until it cuts off the light through both apertures simultaneously. The knife edge is then at the focus of the zone defined by the mask.

Just as for the Hartmann test, it is possible to obtain the wavefront from either the transverse or the longitudinal aberrations. If the slope, β, of the wavefront is calculated from the transverse or longitudinal aberration, numerical integration can be used to calculate the wavefront profile across the wavefront. If β_i and x_i are the slope and real coordinate (not normalized) of the ith point across the wavefront, the wavefront aberration is given by

$$\Delta W = \frac{1}{2}\sum_{i=1}^{n} (\beta_{i-1} + \beta_i)\,(x_i - x_{i-1}) \qquad (9)$$

It should be noted that if both the light source and the knife edge are moved together, as is often the case for testing mirrors, the effective motion of the knife edge is twice the actual motion.

The advantages of the knife edge test are that it is simple and convenient, and no accessory optics are required. Also, the whole surface can be viewed at once, and the test is sensitive. The disadvantages of the test are that it is sensitive to slopes rather than heights, and it measures slopes in a single direction with a single orientation of the knife edge. Because of diffraction, the shadow position can be difficult to define.

One way of improving quantitative measurements performed using the knife edge is to use a phase knife edge instead of a density knife edge. In a phase knife edge both parts of the knife are transparent, but one side introduces a phase difference, preferably 180°. In this case the diffraction pattern produced by the knife edge is symmetric and if the phase difference is exactly 180° the center of the diffraction pattern is dark. The most important feature is that since the diffraction is symmetrical, the center of the pattern can be identified.

8.2.13 Wire Test

The wire test is the same as the Foucault test except the knife edge is replaced with a wire (or slit). Often the wire is a strand of hair. The wire test is inferior to the Foucault test as far as obtaining qualitative data, but it is superior as far as obtaining quantitative data since the wire gives a sharper boundary than the knife edge. Figure 11 shows some computer-generated images that would be obtained using the wire test. The images of the wire are described by the same equations given above for the shadow boundaries in the Foucault test. Figure 12 shows experimental results for using the wire test to evaluate a parabolic mirror at the center of curvature.

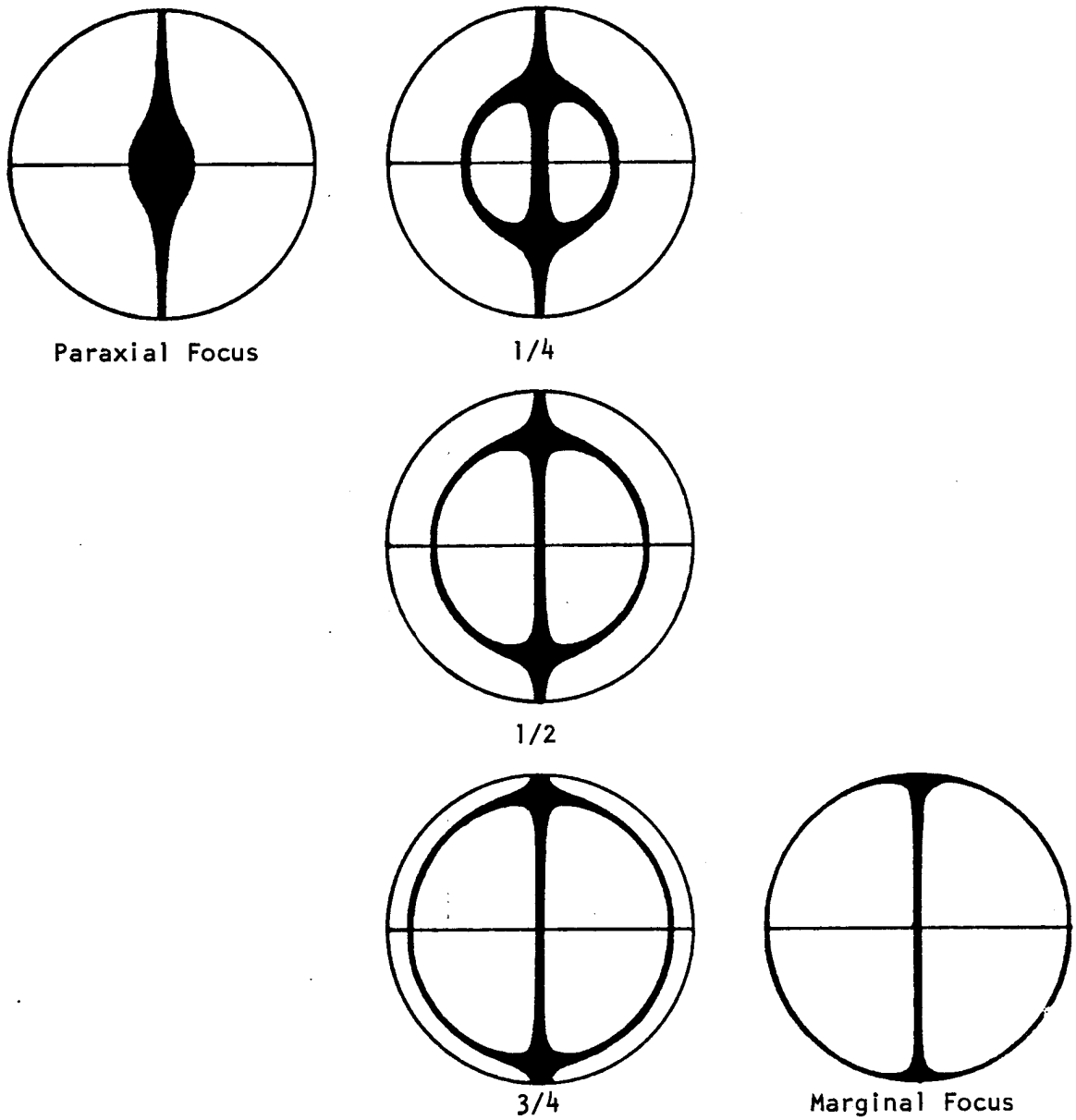

Fig. 11a. Wire test pattern showing effect of focus for third-order spherical aberration (from R. V. Shack).

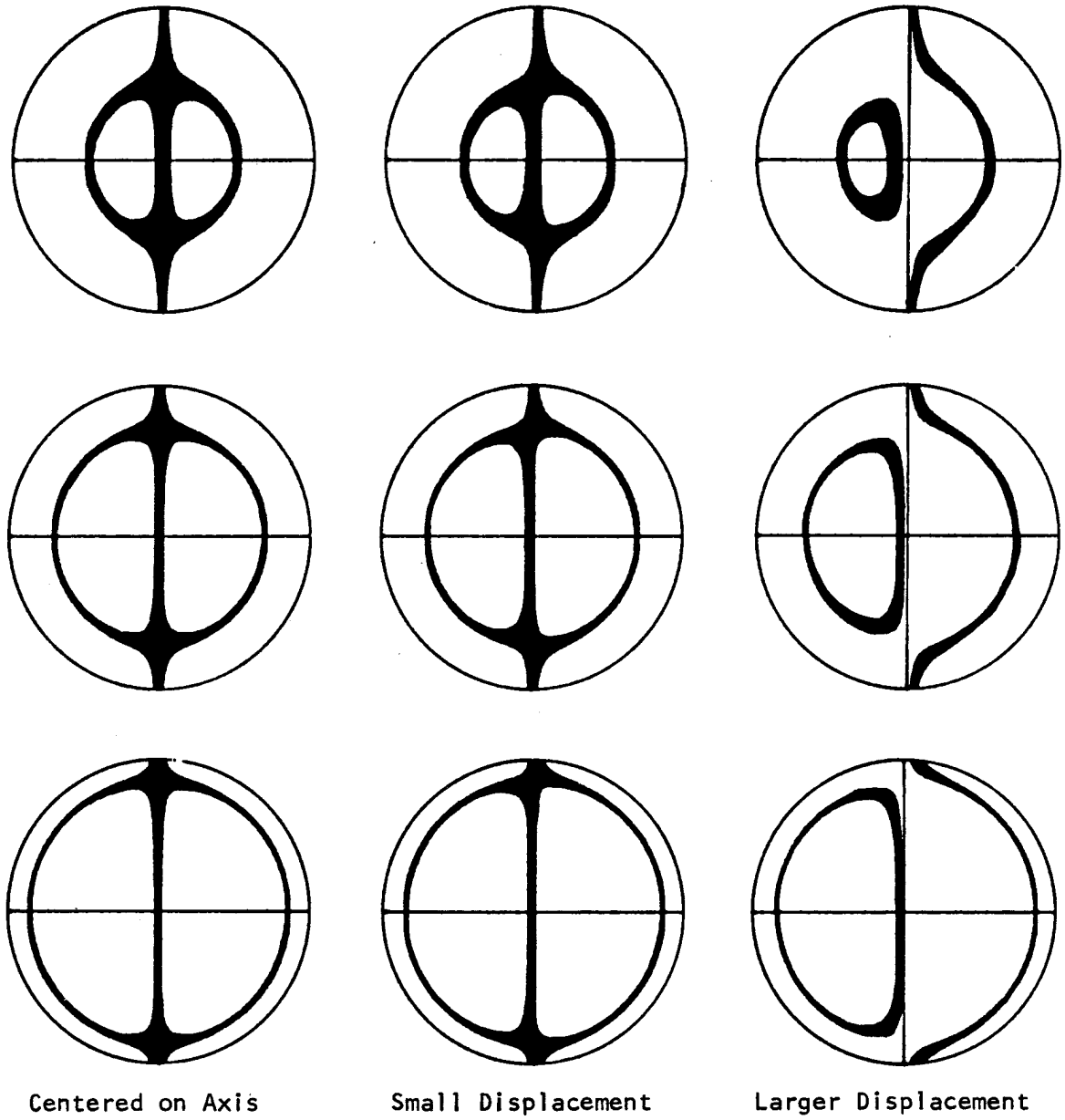

Fig. 5-11b. Wire test pattern showing effect of lateral displacement of wire for third-order spherical aberration (from R. V. Shack).

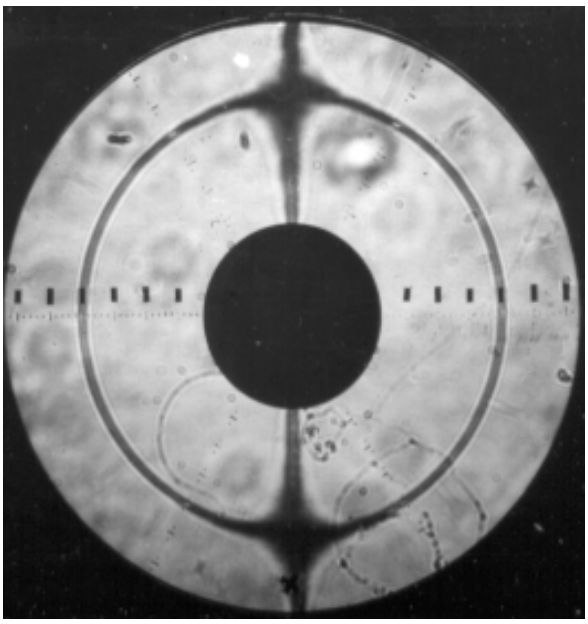

Wire test experimental results for parabolic mirror tested at center of curvature

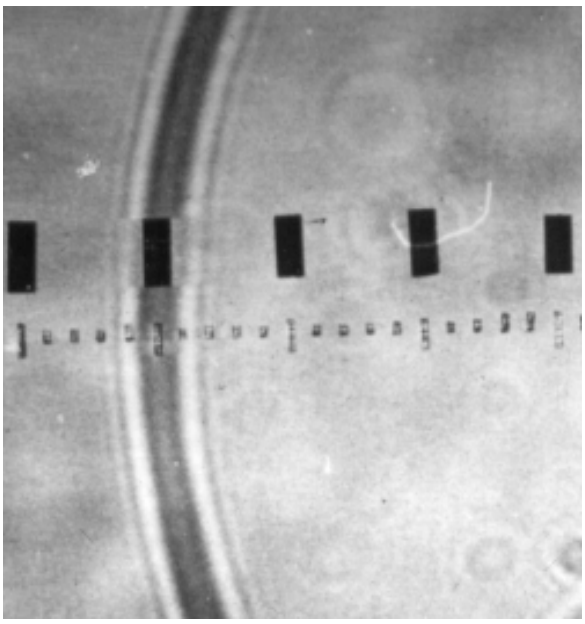

Close-up showing diffraction pattern

Fig. 12. Experimental results obtained using the wire test to evaluate a parabolic mirror at the center of curvature.

8.2.14 Ronchi Test

In the Ronchi test, a low-frequency grating, called a Ronchi ruling, is substituted for the knife edge used in the Foucault test, or the wire used in the wire test. The test may be understood by considering the Ronchi ruling as equivalent to multiple wires. A typical experimental arrangement for utilizing a Ronchi ruling is shown in Fig. 13. Instead of a single wire, we now have several wires to consider, and instead of a single shadow, we now have several shadow boundaries. In our analysis we will initially neglect diffraction.

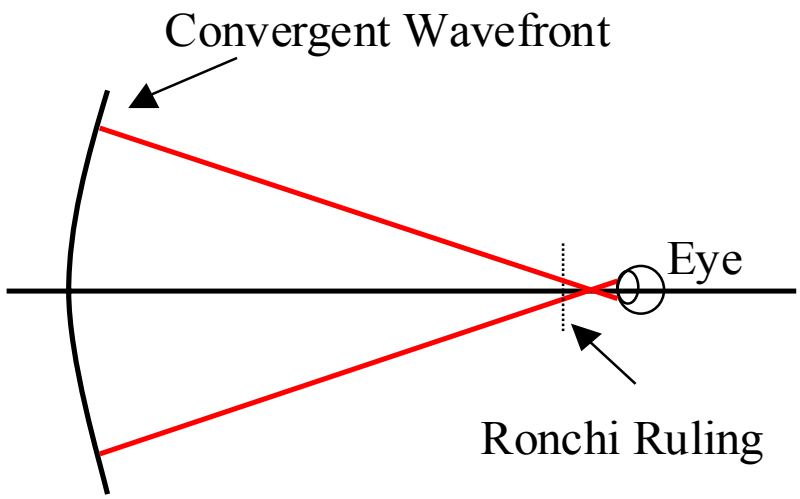

Fig. 13. Ronchi test.

Let the Ronchi ruling be inserted in the beam a distance ϵ_z from the paraxial focus. Suppose the rulings make an angle α with respect to the x axis. If we let d be the grating spacing and m be an integer (which we shall call the order number), then the equation for the shadow boundaries is

$$m\,d = -\epsilon_x \operatorname{Sin}[\alpha] + \epsilon_y \operatorname{Cos}[\alpha] = \frac{R}{h}\frac{\partial \Delta W}{\partial x}\operatorname{Sin}[\alpha] - \frac{R}{h}\frac{\partial \Delta W}{\partial y}\operatorname{Cos}[\alpha] \tag{10}$$

First, consider a perfect lens. If $\alpha = 90°$, then the equation for the shadow boundaries is

$$m\,d = \frac{R}{h}\frac{\partial \Delta W}{\partial x} = -\frac{\epsilon_z h}{R}\,x \tag{11}$$

Hence, the pattern observed in the Ronchi test of a perfect lens is a series of straight lines corresponding to different values of m, as shown in Fig. 14. The number of lines in the field depends upon the distance between the Ronchi ruling and the focus.

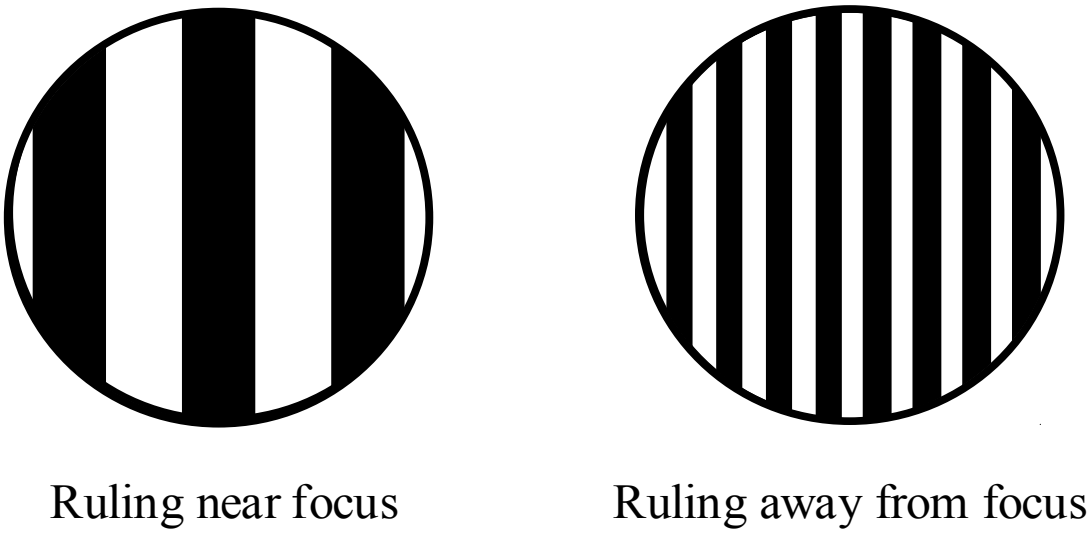

Fig. 14. Ronchi test patterns of a perfect lens.

Let us now consider the situation where the wavefront has third-order spherical aberration. The equation for the shadow boundaries is the same as Eq. (1) given for the Foucault test except now d is replaced with md. Figure 15 gives typical Ronchi test patterns for third-order spherical aberration.

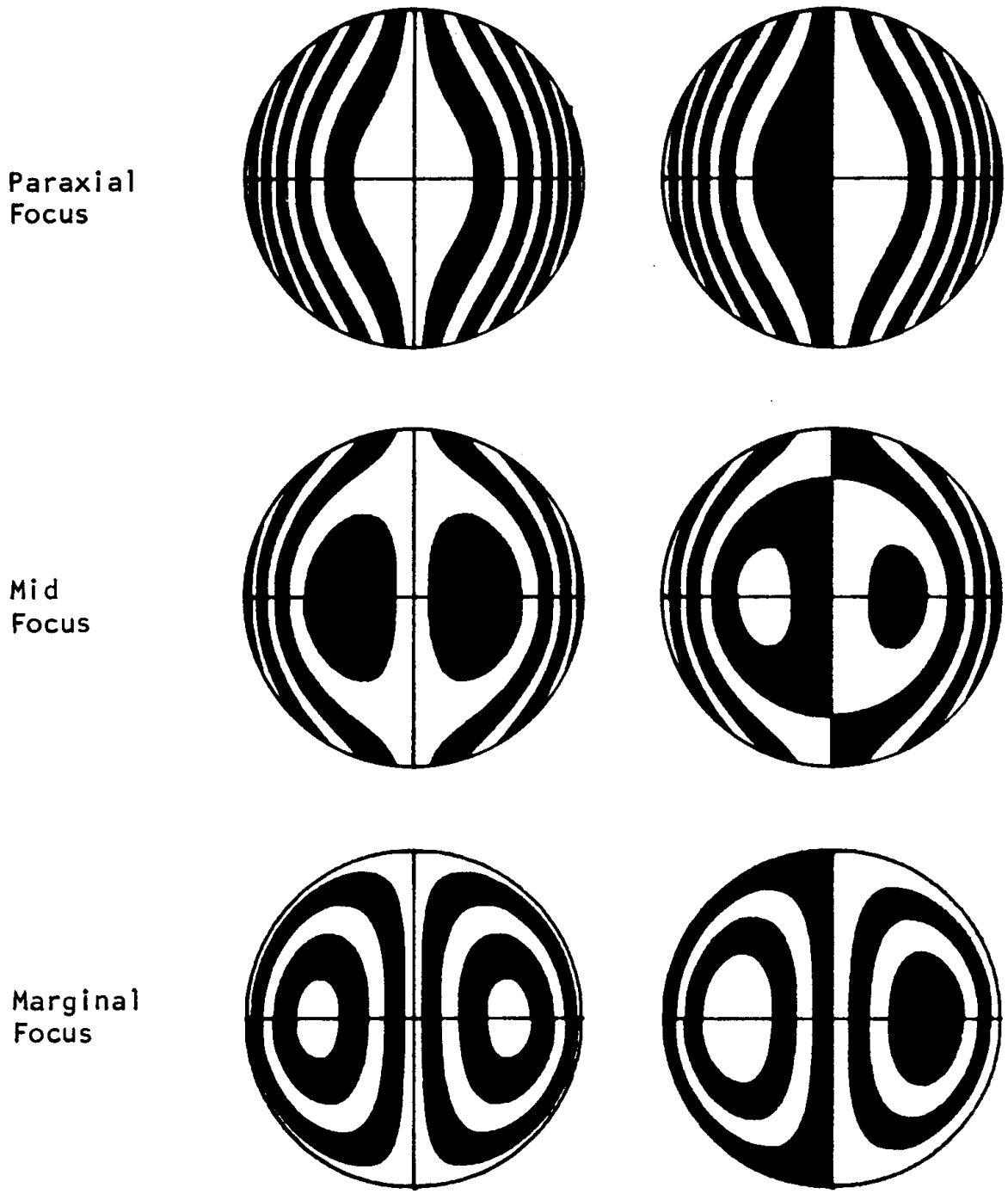

Fig. 5-15. Ronchi test patterns for third-order spherical aberration (from R.V.Shack).

Likewise, the Ronchi pattern for coma is obtained from Eqs. (5) and (6) by replacing d with md. The resulting elliptical and hyperbolic patterns are shown in Fig. 5-16. The behavior of the Ronchi pattern for astigmatism is the same as for the Foucault test described above. Figure 5-17 shows the corresponding pattern of an astigmatic wavefront as the Ronchi ruling is moved through focus.

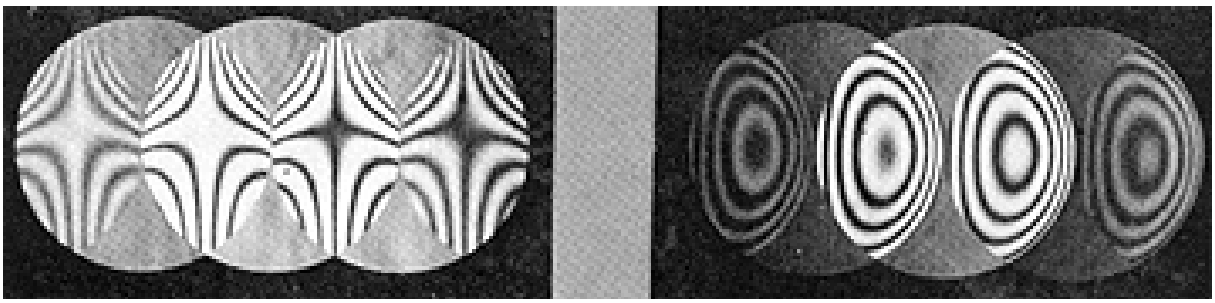

Fig. 5-16. Ronchi test patterns for coma (from V. Ronchi, "Forty Years of History of a Grating Interferometer," Applied Optics 3, 437-451, 1964).

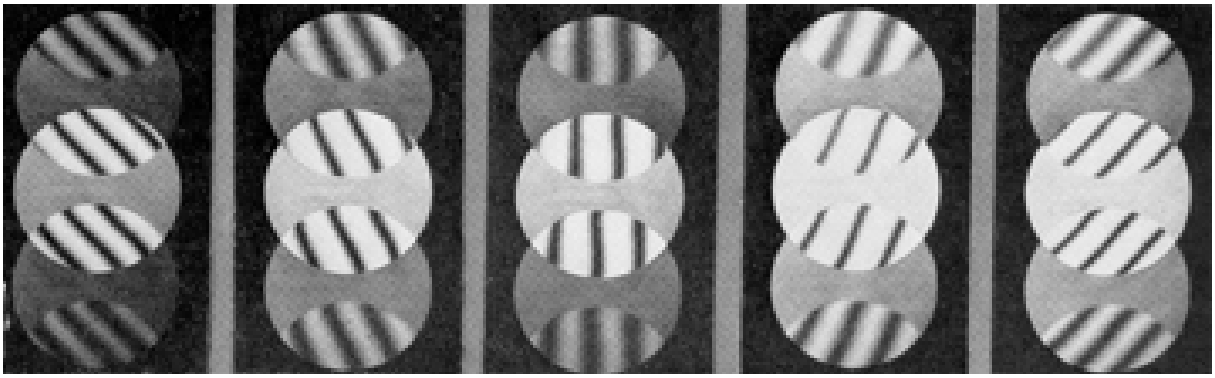

Fig. 5-17. Ronchi test patterns for astigmatism (from V.Ronchi,"Forty Years of History of a Grating Interferometer," Applied Optics 3, 437-451, 1964).

Generally, the Ronchi ruling is not used with a point or slit source, but rather the ruling is illuminated by a diffuse source from behind as shown in Fig. 5-18. The ruling then acts as a multiple slit source, with the light from each opening in the grating producing a test pattern identical to that of the other openings.

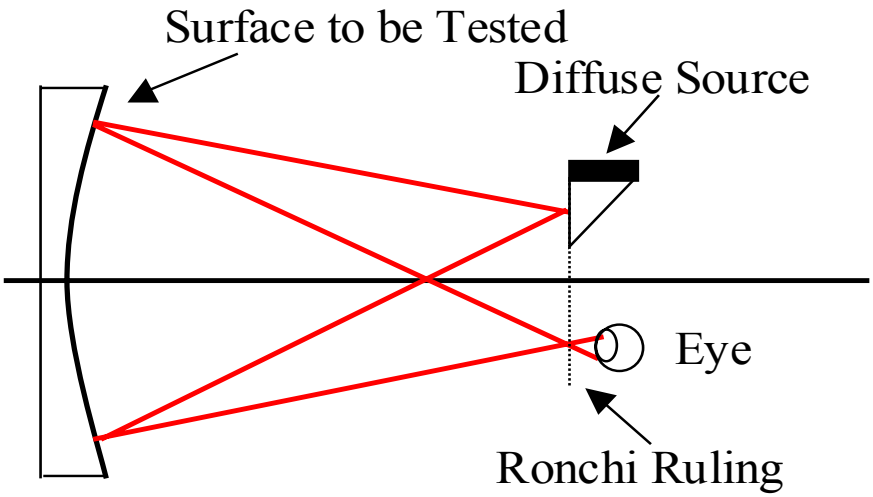

Fig. 5-18. The use of Ronchi rulings with a diffuse source.

Unfortunately, diffraction effects are readily observed when using Ronchi rulings to test optics. In the Ronchi test, the ruling acts as a diffraction grating to create multiple images of the surface being tested. If the gratings are

coarse, say less than l0 lines/mm, the multiple images due to diffraction will lie close together, and will cause only a slight perturbation of the shadow pattern. If high-frequency gratings, say greater than l00 lines/mm are used, the various images of the surface being tested will be clearly distinguished. It can be shown that the patterns obtained in a Ronchi test are essentially the same when the various images of the source are clearly resolved as they are when diffraction can be totally neglected. In the intermediate situation where the various images of the test surface all overlap, the resultant patterns are difficult to analyze.

The advantages of a Ronchi test are that the test is simple and will work with a white light source. The disadvantage is that it does not give the wavefront directly, and for a single Ronchi ruling orientation, slope in only one direction is obtained. Also, the diffraction effects are very troublesome and limit the accuracy of the test.